crystals

MDPI

Article

The Influence of a Commercial Few-Layer Graphene on Electrical Conductivity, Mechanical Reinforcement and Photodegradation Resistance of Polyolefin Blends

S. M. Nourin Sultana [1], Emna Helal [1,2], Giovanna Gutiérrez [2], Eric David [1], Nima Moghimian [2] and Nicole R. Demarquette [1,*]

[1] Mechanical Engineering Department, Ecole de Technologie Superieure, 1100 Notre-Dame Street West, Montreal, QC H3C 1K3, Canada
[2] NanoXplore Inc., 4500 Thimens Blvd, Saint-Laurent, QC H4R 2P2, Canada
* Correspondence: nicoler.demarquette@etsmtl.ca

Abstract: This work demonstrates the potentials of a commercially available few-layer graphene (FLG) in enhancing the electro-dissipative properties, mechanical strength, and UV protection of polyolefin blend composites; interesting features of electronic packaging materials. Polyethylene (PE)/ polypropylene (PP)/ FLG blend composites were prepared following two steps. Firstly, different concentrations of FLG were mixed with either the PE or PP phases. Subsequently, in the second step, this pre-mixture was melt-blended with the other phase of the blend. FLG-filled composites were characterized in terms of electrical conductivity, morphological evolution upon shear-induced deformation, mechanical properties, and UV stability of polyolefin blend composites. Premixing of FLG with the PP phase has been observed to be a better mixing strategy to attain higher electrical conductivity in PE/PP/FLG blend composite. This observation is attributed to the influential effect of FLG migration from a thermodynamically less favourable PP phase to a favourable PE phase via the PE/PP interface. Interestingly, the addition of 4 wt.% (~2 vol.%) and 5 wt.% (~2.5 vol.%) of FLG increased an electrical conductivity of ~10 orders of magnitude in PE/PP—60/40 (1.87×10^{-5} S/cm) and PE/PP—20/80 (1.25×10^{-5} S/cm) blends, respectively. Furthermore, shear-induced deformation did not alter the electrical conductivity of the FLG-filled composite, indicating that the conductive FLG network within the composite is resilient to such deformation. In addition, 1 wt.% FLG was observed to be sufficient to retain the original mechanical properties in UV-exposed polyolefin composites. FLG exhibited pronounced UV stabilizing effects, particularly in PE-rich blends, mitigating surface cracking and preserving ductility.

Keywords: graphene; polyolefin; electrical conductivity; photoprotection; mechanical properties

Citation: Sultana, S.M.N.; Helal, E.; Gutiérrez, G.; David, E.; Moghimian, N.; Demarquette, N.R. The Influence of a Commercial Few-Layer Graphene on Electrical Conductivity, Mechanical Reinforcement and Photodegradation Resistance of Polyolefin Blends. *Crystals* **2024**, *14*, 687. https://doi.org/10.3390/cryst14080687

Academic Editor: Conrad Becker

Received: 12 June 2024
Revised: 20 July 2024
Accepted: 24 July 2024
Published: 27 July 2024

1. Introduction

Currently, the incorporation of carbonaceous filler [1–9] in the polymer matrix is a promising field of research, aiming at the improvement of the properties of polymers. Among these carbon-based fillers, carbon black is zero-dimensional, carbon nanotube is one-dimensional, and graphene is two-dimensional [10]. Due to the two-dimensional geometry of graphene, the extent of dermal effect, inhalation problem, and gene toxicity associated with graphene is much less than that of carbon black or carbon nanotube [11]. This ensures the safer handling of graphene. Moreover, graphene [12] stands out as a highly promising candidate. Theoretically, sp^2-hybridized carbon atoms are arranged in a hexagonal lattice within atomic thickness to form pristine graphene [13]. This unique structure offers remarkable characteristics. A perfect single-layer graphene is not only the lightest (weighing merely 0.77 milligrams per square meter) but also the strongest (300 times stronger than Kevlar) nanofiller discovered to date [14]. Furthermore, graphene demonstrates exceptional electrical and thermal conductivity, along with remarkable flexibility,

capable of stretching up to 25% of its original length without fracturing. These remarkable attributes refer to graphene as a wonder material with the capability of enhancing its properties (processability [15], photostability [16], mechanical [17], and electrical [18]) of polymer composites.

In general, graphene has been observed to enhance the tensile strength and stiffness of polymeric systems, often at the expense of ductility and impact strength [17–19]. Nevertheless, some exceptional observations can be found in the literature [20,21]. Due to graphene's intrinsic electrical conductivity, it can significantly improve the electrical conductivity of polymer composites [22,23]. Furthermore, polymer blend composites often exhibit an even higher electrical conductivity than single polymer/conductive filler composites. This is attributed to the double percolation effect [24–29], which is achievable in co-continuous polymer blend composites. Moreover, the migration of electrically conductive filler from one phase to another via the polymer phase interface (achievable via strategic mixing conditions) can also facilitate the improvement of electrical conductivity in polymer blend composites [30].

Numerous studies [31–34] have investigated the influence of laboratory-processed graphene on the mechanical and electrical properties of various polymer composites. However, the large-scale production of very pure and fully exfoliated graphene is challenging [35]. In contrast, mass production of few-layer graphene (FLG) is obtainable following the cost-effective mechanochemical exfoliation of graphite [36], which involves a lower carbon footprint in comparison to mass production of carbon black [37]. Despite exhibiting a wider size distribution and increased defects compared to lab-grade graphene, particles produced through this process still retain many of graphene's notable properties. Accordingly, better electrical conductivity, improved mechanical strength, and improved photostability of commercial-grade few-layer graphene-filled (FLG) polymer composites have been reported in the literature [16,38]. Nevertheless, research aiming to achieve a combination of improved electrical conductivity, mechanical strength, and photoprotection in the same polymer blend composite remains limited in the literature.

In this connection, polyolefin systems were chosen due to their versatility in domestic and industrial applications. Moreover, approximately 50% of global plastic waste is composed of PE/PP mixtures [39]. A significant portion of this plastic waste can be recovered as a PE/PP mixture from post-consumer waste using simple separation steps. However, further separating PE from PP is both complex and costly [40]. This motivates research into enhancing the properties of controlled PE/PP blend systems to gain a deeper understanding. Such knowledge could be valuable in guiding the upcycling of polyolefin mixtures recovered from post-consumer waste. In this study, polyethylene (PE), polypropylene (PP), and PE/PP blend systems were selected to explore the potential of incorporating commercially available FLG. Different concentrations of FLG were melt-mixed with PE, PP, and PE/PP blend systems. For the PE/PP blend system, two different FLG mixing strategies were employed to investigate their influence on the electrical properties of the composite. However, if the filler fails to stabilize the morphology, subsequent morphological evolution during post-processing is a likely phenomenon for an immiscible polymer blend composite. Shear-induced deformation followed by small-amplitude oscillatory shear (SAOS), a rheological approach [41], was conducted to study the morphological stability/evolution of the PE/PP/FLG blend composite. After the deformation step, SAOS was performed to reach an equilibrium state of the deformed morphology. A similar approach has been extensively studied for droplet-dispersed type polymer blend systems [42]. Furthermore, the influence of adding FLG on the mechanical properties of the composites before and after UV exposure was documented.

2. Materials and Methods

2.1. Materials

GrapheneBlack 3X, a few-layer (6 to 10) graphene powder, was received from NanoXplore Inc., Montreal, QC, Canada, to prepare the composites for this study.

Two homopolymers, high-density polyethylene (HDPE) and polypropylene (PP), were used as the thermoplastic components of the composites. Table 1 outlines the specifications of the polymers.

Table 1. Identification, MFI, and density of the polymers used in this work.

Polymer	Commercial Name	MFI (g/10 min)	Density (g/cm^3)
HDPE	Alathon H5618	17 (190 °C, 2.16 kg)	0.955
PP	Polypropylene 3720 WZ	20 (230 °C, 2.16 kg)	0.905

2.2. Methods

To prepare the composites for this study, master batch (MB) pellets of either PE/FLG or PP/FLG were used for the preparation of composites. The MB pellets contained 30 wt.% FLG, provided by NanoXplore, Inc. The samples were produced by using a HAAKE twin-screw extruder (Rheomex OS PTW16/40).

PE and PP were separately blended at 200 °C and 150 rpm with their respective MB pellets to create the PE/FLG and PP/FLG composites. Each composite consisted of 1 and 5 wt.% of FLG, respectively.

In addition, PE/PP—20/80 and PE/PP—60/40 blend composites with the FLG concentration ranging from 1 to 5 wt.% were prepared in two steps. First step: PE/FLG or PP/FLG MB pellets were blended with PE or PP at 200 °C and 150 rpm, referred to as the premixing step. Second step: these premixtures were melt-blended with the other respective polymer blend at 190 °C and 115 rpm.

Finally, extruded pellets were injection molded in an Arburg Allrounder 221K-350-100 Injection molding machine to prepare dog-bone-shaped specimens and rectangular specimens for the characterization of tensile and impact properties, respectively. During injection molding, a certain temperature profile (zone 1: 175 °C, zone 2—180 °C, zone 3—180 °C, zone 4—180 °C, zone 5—185 °C) was followed at a 0.3 in^3/sec injection speed and 8500 Psi injection pressure. It is worth mentioning that the injection duration was 30 s, pressing was continued for 5 s, clamping pressure was maintained at 1000 psi, and the injected samples were cooled for 25 s while the mold temperature was maintained at 70 °C.

Moreover, disks of 1 mm thickness and 25 mm diameter were prepared by compressing the composites at 200 °C and 10 MPa for 10 min in a compression mold.

2.3. Photodegradation Process

The injection-molded composites were weathered in a QUV chamber. The samples were treated under UV radiation for a total of 2 weeks and 4 weeks by following the alternating two steps mentioned in Table 2.

Table 2. Weathering conditions of the specimens in QUV chamber.

Step	Function	Irradiance (W/m^2)	Temperature (°C)	Time (h:m)
1	Exposure to UV radiation	0.89	60	8:00
2	No UV radiation	n/a	50	4:00

2.4. Characterizations

Scanning electron microscope (SEM) images were captured by using a Hitachi SEM S3600-N (Model: MEB-3600-N, manufactured by Hitachi Science Systems, Ltd., Tokyo, Japan). Prior to SEM imaging, the surface (cryo-fracture or UV exposed) of the samples was gold coated by employing a Gold Sputter Coater (Model: K550X, manufactured by Quorum Technologies Ltd, East Sussex, Lewes, UK).

The electrical conductivity of the composites was assessed using a broadband dielectric spectrometer (BDS) from Novocontrol Technologies GmbH & Co. KG, Montabaur, Germany.

The investigation was conducted under an excitation voltage of 3 VRMS across a frequency range from 1×10^{-2} to 3×10^{5} Hz. Gold-coated disk-shaped composites of 1 mm thickness were sandwiched between two brass disks (electrodes) of 25 mm diameter in order to create a plane capacitor structure for the analysis of the electrical properties. The real part of the complex electrical conductivity at the lowest frequency (1×10^{-2} Hz) has been reported as the electrical conductivity of the composite in the subsequent section of this study.

Shear-induced coalescence followed by SAOS was conducted on the rheometer, MCR 501. Compression-molded neat and FLG-filled PE/PP—20/80 composites were sheared at 0.05 s^{-1} rate for 500 s, 2000 s, and 5000 s, respectively. In other words, the samples were deformed at 25, 100 and 250 strains (shear rate × duration), respectively. After each extent of deformation, the sample was subjected to SAOS for stabilization of the deformed morphology, and the sample was saved for further investigation. A schematic representation of the rheological approach has been provided in Figure 1. The shear rate (0.05 s^{-1}) was chosen low enough to favor coalescence. This shear rate was selected based on the critical capillary number (a function of the viscosity ratio of the dispersed matrix phase, the viscosity of the matrix phase, the interfacial tension and the average droplet size). Relevant theory [43,44], the calculation of the critical capillary number, and the selection of the shear rate to investigate the morphological evolution are provided in the Supplementary section of this work. It is worth mentioning that the deformed samples were saved and cryo-fractured, followed by a gold coating to investigate the resultant morphology using SEM images.

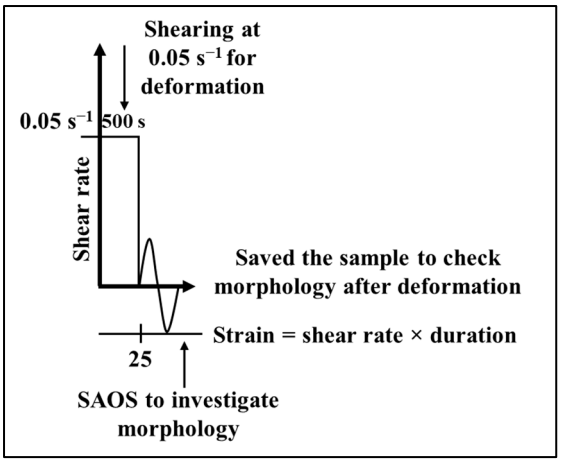

Figure 1. A schematic representation of the shear deformation followed by SAOS, a rheological approach, to study the morphological evolution of neat and FLG-filled PE/PP blends. A similar approach was followed for 2000 s and 5000 s, respectively.

The tensile properties were characterized according to ASTM D638 at room temperature with a 10 kN load cell and a crosshead speed of 50 mm/min. The MTS Alliance RF/200 tensile test apparatus was used for the investigation of tensile property. Dog-bone-shaped samples with 160 mm length, 12 mm width, and 3.5 mm thickness were used to characterize the tensile properties of the samples.

The Izod (notched) impact strength was investigated according to ASTM D256 by using the impact strength tester device (manufactured by International Equipments, Maharashtra, India). Prior to the test, a notch was created on each sample (62 mm × 12 mm) by using a motorized notch cutter, manufactured by International Equipments, India.

At least five replicas were considered for each sample to investigate mechanical properties, and the average value has been reported along with the standard deviation (SD) as an error bar.

A Perkin-Elmer FTIR spectrometer(manufactured by PerkinElmer, Wales, UK), specifically the Spectrum Two™ model equipped with a diamond crystal, was utilized for capturing the Attenuated total reflectance-Fourier transform infrared spectroscopy (ATR-FTIR)

spectrum. Thin films collected from the surface of both neat and FLG-filled composites (both pre- and post-UV exposure) were analyzed to obtain their respective FTIR spectra. Each spectrum comprised 10 scans and was collected at a resolution of 4 cm^{-1} across the wave number range of 400–4000 cm^{-1}.

FTIR spectra were utilized to investigate the relative carbonyl content of each sample, employing Equation (1)

$$\text{Relative carbonyl content} = \frac{A_{C=O} \text{ after UV exposure}}{A_{C=O} \text{ before exposure}} \quad (1)$$

In this context, $A_{(C=O)}$ denotes the area under the peak (within the wave number range of 1680–1800 cm^{-1}), indicative of the C=O functional group [16]. FTIR spectra of samples before and after UV exposure can be found in the Supplementary Materials (see Figure S1a–e). Evaluating the relative carbonyl content is of interest as it serves as an indicator of polymer degradation over time. To ensure accuracy, a minimum of three spectra from distinct regions of the samples were analyzed to compute and present the average carbonyl content values.

3. Results and Discussion

3.1. Morphology of Neat Blends

Figure 2a–c illustrate the microstructure of neat PE/PP blends with ratios of 20/80, 60/40, and 80/20, respectively. All the blends presented a droplet-dispersed morphology. However, droplet phase and size are governed by the blend composition. For instance, the PE/PP—20/80 blend represents PE droplets in the PP matrix. In contrary, PE/PP—60/40 and PE/PP—80/20 blends show PP droplets dispersed in the PE matrix. However, PP droplet size is bigger in PE/PP—60/40 than that of PE/PP—80/20. This size difference is attributed to the higher proportion of the PP phase (minor phase) in the PE/PP 60/40 blend system. The presence of a comparatively higher portion of the minor phase in an immiscible polymer blend increases the probability of droplet coalescence. This phenomenon may result in bigger droplets in the matrix phase.

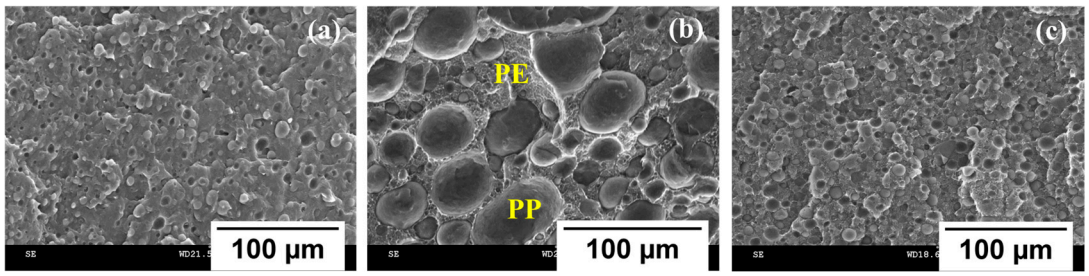

Figure 2. SEM images of PE/PP blends: (**a**) PE/PP—20/80, droplets representing PE phase; (**b**) PE/PP—60/40, droplets representing PP phase; (**c**) PE/PP—80/20, droplets representing PP phase.

3.2. Influence of FLG on Morphology of Blend Composite

Figure 3 illustrates the distribution of PP droplet size (number average droplet radius, R_N) in a neat and FLG-filled PE/PP—20/80 blend composite. The addition of FLG results in a reduced and narrower distribution of PE droplet size. The addition of 2 wt.% and 5 wt.% of FLG results in a notable reduction in droplet size. The formation of finer morphology is attributed to the inhibition effect of rigid filler against the coalescence of droplets to grow bigger. A similar effect of rigid fillers was reported in the literature [45].

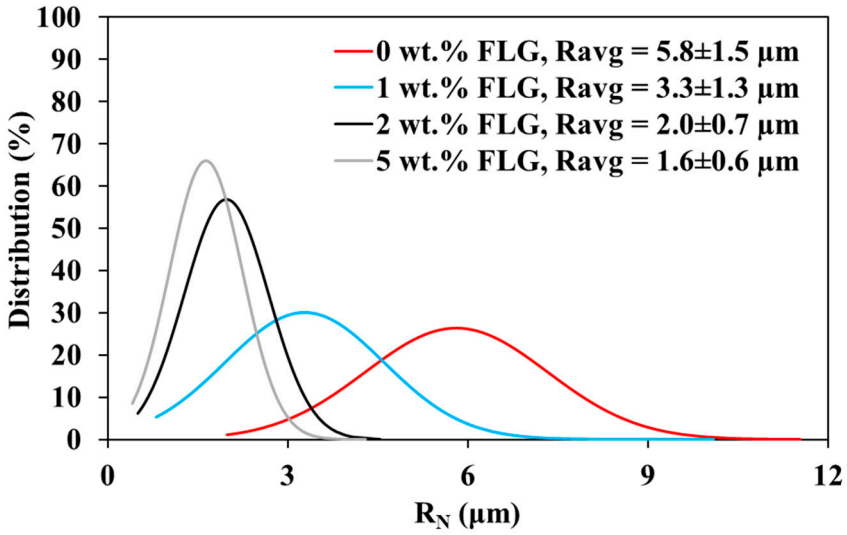

Figure 3. Distribution of PE droplet size in neat and FLG-filled PE/PP—20/80 blend composite with 1, 2 and 5 wt.% of FLG, respectively.

The SEM micrographs in Figure 4a–c depict the influence of the addition of 5 wt.% of FLG on the microstructure of PE/PP blend composites. The introduction of FLG causes deformation of PE droplets in PE/PP—20/80 and PP droplets in PE/PP—60/40 and PE/PP—80/20 blends, respectively. Particularly in the PE/PP—60/40 blend, the deformation of relatively larger PP droplets enhances the likelihood of continuity in the minor PP phase. This phenomenon, in turn, can facilitate the creation of an uninterrupted network of electrically conductive fillers in the polymer blend composite.

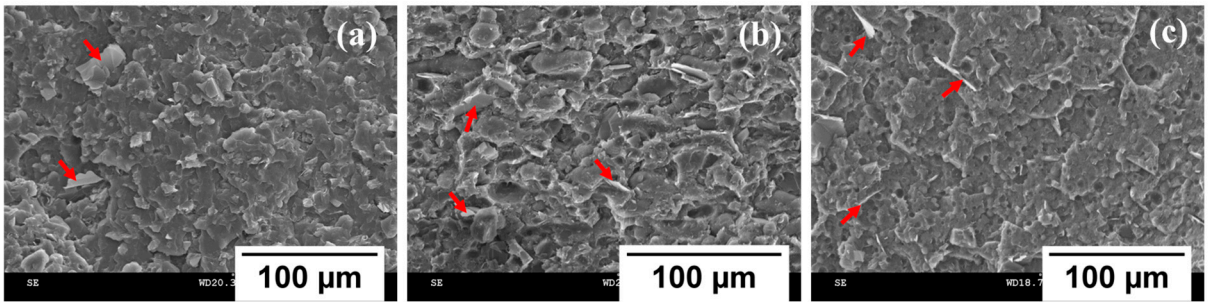

Figure 4. SEM images of the phase morphology of 5 wt.% FLG-filled composites; (**a**) PE/PP—20/80; (**b**) PE/PP—60/40 and (**c**)PE/PP—80/20. The red arrows are used to indicate the presence of FLG in the composites.

3.3. Influence of FLG on Electrical Conductivity of Composites

The impact of different FLG mixing strategies has been studied (see Figure S2 in the Supplementary Materials) on the electrical conductivity of a PE/PP—60/40 blend composite. Notably, the composite exhibits significantly higher electrical conductivity when FLG is pre-mixed with the PP phase compared to when it is pre-mixed with the PE phase. This observation motivated us to carry on the rest of the study with composites, where FLG was pre-mixed with the PP phase. Figure 5 reports the change in electrical conductivity in FLG-filled composites with different concentrations of FLG in the composites. The graph displays that the electrical conductivity of PE/PP—60/40 blend composite is higher than that of PE/PP—20/80 blend composite, specifically up to 4 wt.% of FLG. However, when the FLG concentration reaches 5 wt.%, both blend composites demonstrate similar electrical conductivity. This suggests that the electrical properties are significantly influenced by the morphology, governed by blend compositions. In contrast, FLG-filled PE, PP, and PE/PP—80/20 remain insulative, even at a dosage of 5 wt.% FLG. Notably, the PP/FLG

composite exhibits higher electrical conductivity than that of PE/FLG at 9 wt.% concentration of FLG. This observation implies that a relatively lower concentration of FLG is required in the PP matrix compared to the PE matrix to establish a continuous FLG network.

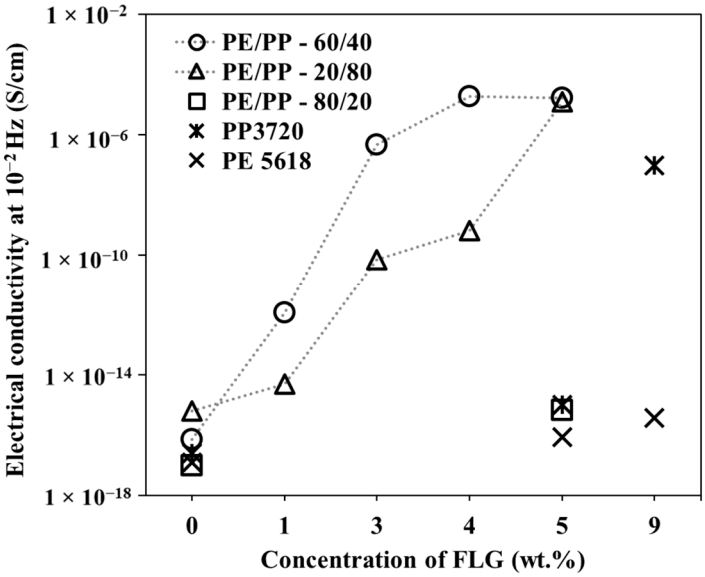

Figure 5. Real part of the conductivity of the compounds at 10^{-2} Hz (the lowest frequency) for different concentrations of FLG. Dotted lines are used to guide the reader's eye.

3.4. Influence of Deformation on Electrical Conductivity of Blend Composite

Figure 6 presents the electrical conductivity of the deformed PE/PP—20/80 blend composite, containing 5 wt.% FLG, as a function of the frequency of the applied electric field. After deforming the composite in molten condition in the Rheometer, the samples were preserved to investigate the electrical conductivity. Intriguingly, despite the deformation in morphology (discussed using Figure S3 in the Supplementary Materials) and a change in filler localization (see Figure S4 in the Supplementary Materials), the electrical conductivity of the composite remained unchanged. This underscores the robustness of the FLG network in withstanding mechanical deformation in molten conditions. This observation is in agreement with the observation reported in the literature [46].

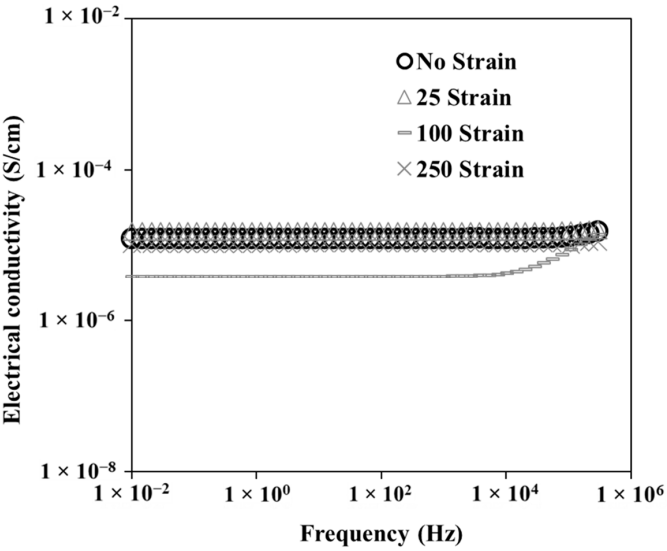

Figure 6. Electrical conductivity of PE/PP -20/80 blend composite (containing 5 wt.% FLG) after deformation by different strains, as a function of frequency.

3.5. Influence of FLG on Mechanical Properties Polyolefin Composites

In Figure 7a–c, the mechanical properties of the samples are plotted as a function of FLG concentration. Since the ductility of PE is around 10 times higher than that of neat PP, the ductility of PE has been plotted on the secondary axis of Figure 7c with different concentration of FLG. Figure 7a illustrates that the tensile modulus of neat PP is higher than that of neat PE. In addition, the tensile moduli of PE, PP, and PE/PP blends are increased by the additions of FLG. It is worth mentioning that the tensile strength of the samples as a function of the concentration of FLG has been provided in Figure S5 in the supplementary materials. The stiffness of polymeric materials can be increased due to the reinforcement effect of rigid fillers. Analogous findings can be observed in the literature [47,48]. Figure 7b shows that the impact strength of PE, PP, and PE/PP blend composites was not significantly affected by the presence of FLG. A similar effect of rigid filler on the impact strength of polymer material was reported earlier [49]. However, Figure 7c shows that the addition of FLG decreased the ductility of the composites. The reduction in elongation at break of PE and PE/PP—60/40 (PE- rich blend) composites is statistically more significant than that of PP and PE/PP—20/80 (PP- rich blend) composites. The presence of rigid filler hinders the polymer chain mobility, which ultimately affects the ductility of the composite. Several works in the literature have reported similar findings [2,17,19].

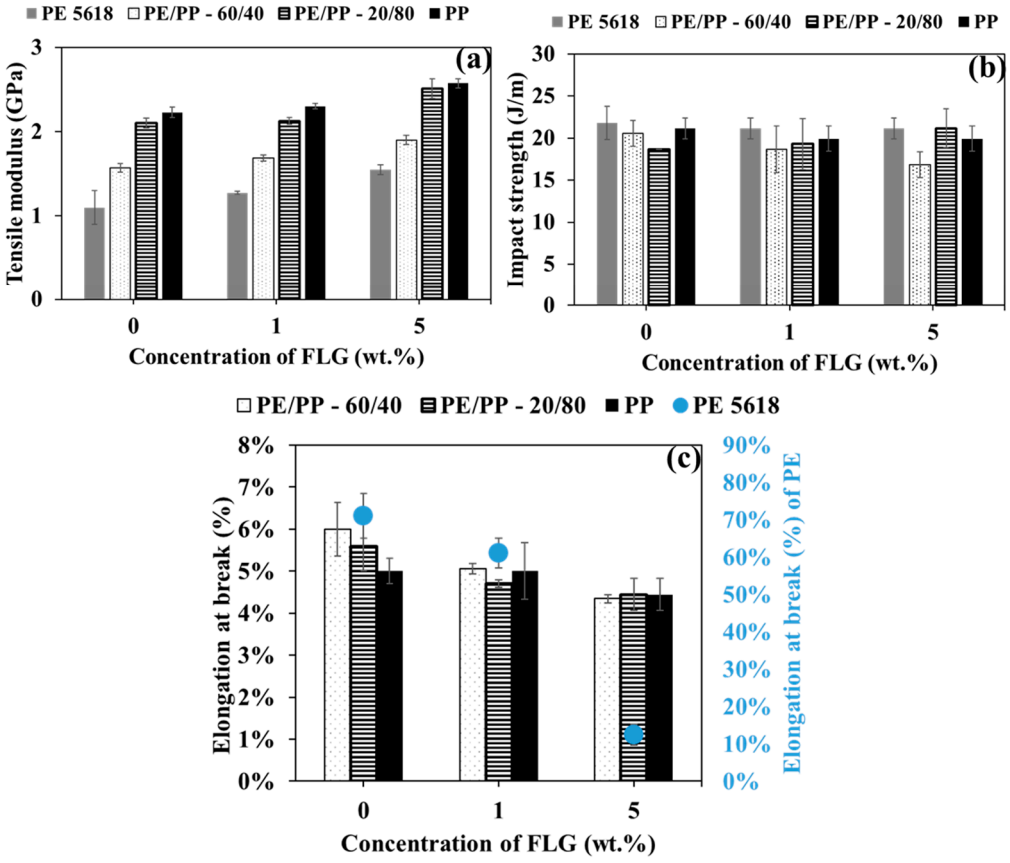

Figure 7. Mechanical properties of: (**a**) tensile modulus, (**b**) impact strength, and (**c**) elongation at break of PE, PE/PP blends, and PP composites with different concentration of FLG.

3.6. Effect of Adding FLG on UV-Exposed Composites

3.6.1. Property Retention of UV-Degraded Composites

In Figure 8, the retention of elongation at break (a sensitive property to UV degradation) after 4 weeks of UV exposure for neat and FLG-filled PE, PE/PP—60/40, PE/PP—20/80, and PP is plotted as the FLG concentration was varied in the composites. The figure illustrates that UV-exposed unfilled PE, PP, and PE/PP blends become

too brittle to capture the correct elongation at break under the testing condition. This indicates a substantial UV degradation of the pure polyolefins. Conversely, FLG-filled polyolefin composites exhibit enhanced retention of ductility under UV radiation, owing to the photoprotective properties of FLG. Nevertheless, this photoprotective effect of FLG is more pronounced in polymeric systems where PE is the predominant phase compared to those where PP is the major component. Further analyses have been carried out in terms of sample surface imaging and FTIR investigation.

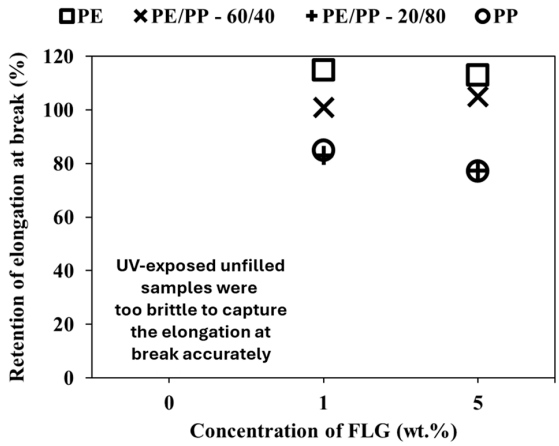

Figure 8. Retention of elongation at break of UV-exposed PE, PE/PP blends, and PP as the FLG concentration increased in the specimens.

3.6.2. Appearance of the Compounds after UV Exposure

The SEM images in Figure 9a–c illustrate the surfaces of neat PE, PE/PP—60/40 blend, and PP samples, which were exposed for 4 weeks under UV radiation. Figure S6 has been provided in the Supplementary section to extend the idea of the appearance of a polyolefin sample before UV exposure. Additionally, Figure 9d–f display the UV-degraded surfaces of PE, PE/PP—60/40 blend, and PP composites, containing 1 wt.% FLG, respectively. Apparently, the presence of FLG lessens the occurrence of UV degradation-driven cracks in the samples' surface compared to their neat counterparts. This suggests that FLG can mitigate the UV degradation process in polyolefins.

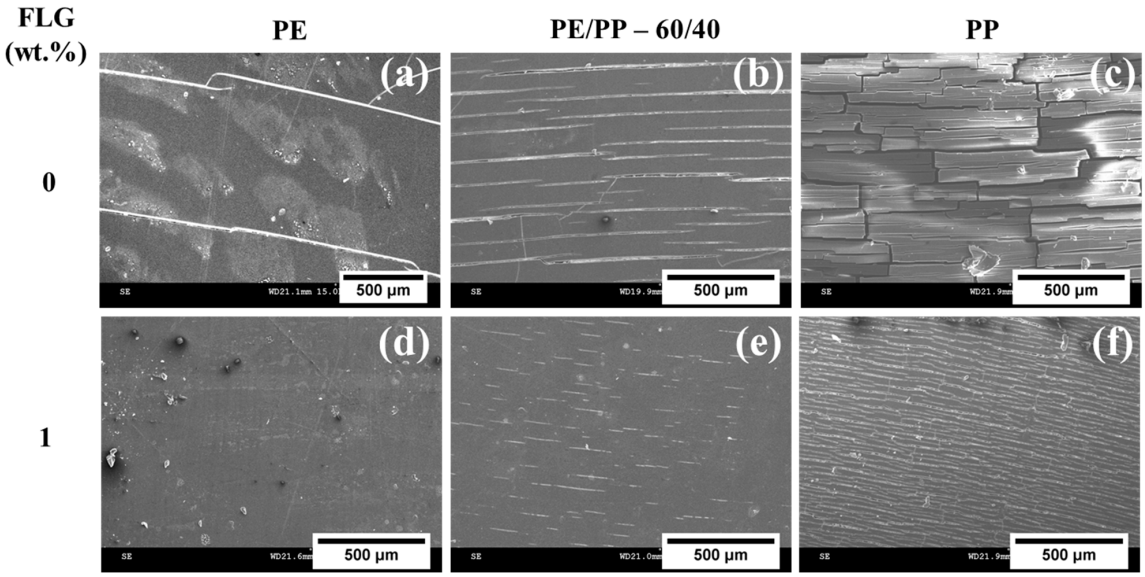

Figure 9. SEM micrographs of the UV-exposed unfilled (**a**) PE, (**b**) PE/PP—60/40, and (**c**) PP along with 1 wt.% FLG-filled (**d**) PE, (**e**) PE/PP—60/40 and (**f**) PP composites.

3.7. Chemical Analysis

In Figure 10, the relative carbonyl content of UV-exposed samples of PE, PE/PP—60/40, PE/PP—20/80 blends, and pure PP, both without and with FLG, is plotted against exposure time. The relative carbonyl content is determined by analyzing the FTIR absorption spectra of each UV-exposed sample and normalizing them against the carbonyl content of the corresponding sample prior to UV exposure. The incorporation of FLG reduces the formation of carbonyl content in UV-exposed composites, indicating the UV-stabilizing effect of FLG in polyolefin systems.

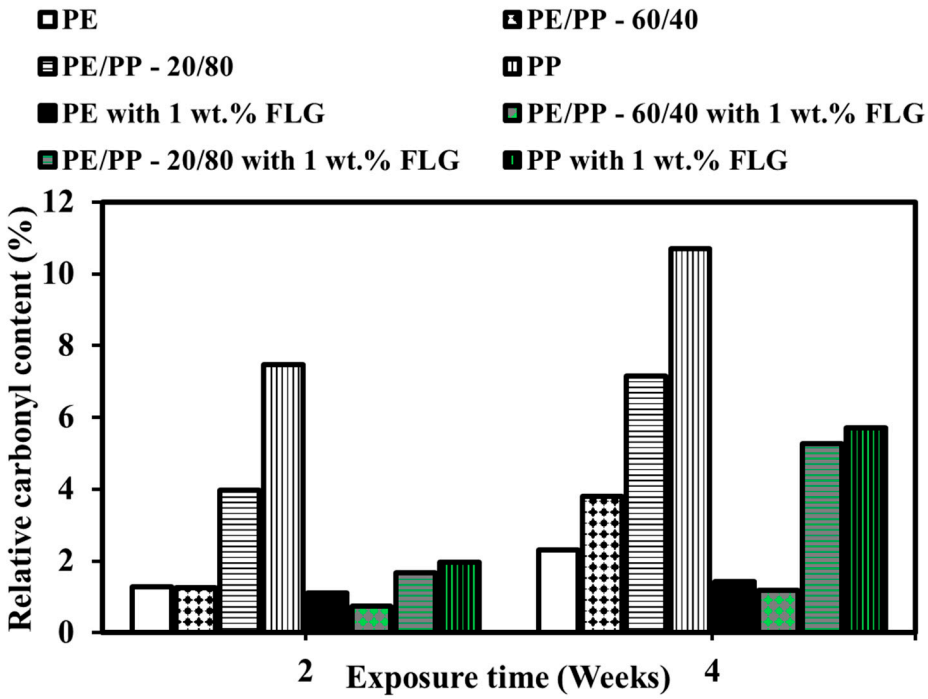

Figure 10. The change in the relative carbonyl content of UV-exposed PE, PE/PP blends, and PP samples with the duration of the UV exposure.

Furthermore, it is evident that the relative carbonyl content in UV-exposed PP is significantly higher compared to that in PE, suggesting that PP is more susceptible to UV degradation than PE. This tendency towards UV degradation is also observed in PE/PP blends; blends with a higher proportion of PP exhibit greater susceptibility to UV degradation compared to those with more PE. An explanation has been extended in the discussion part. Figure 10 illustrates the order of UV degradation tendency in the PE/PP polymer system as follows: PP > PE/PP—20/80 > PE/PP—60/40 > PE. A similar order of UV degradation tendency is noted in FLG-filled PE/PP composites, but the degradation rate is slower, attributed to the UV-stabilizing effect of FLG.

3.8. Discussion

The comprehensive analysis of the morphology, electrical properties, mechanical properties, and UV degradation behavior of FLG-filled PE/PP blend systems provides valuable insights into the multifaceted effects of FLG on polyolefin blend systems.

In a filler-filled, immiscible polymer blend system, double percolation [24–29] is an interesting phenomenon. This phenomenon refers to the percolation of one phase through another phase with the concomitant formation of a filler network through one of the percolating phases. In the case of a conductive filler, the double percolation effect increases the electrical conductivity of the composite by a significant order of magnitude. In this work, Figure 4b shows that the PP phase was not percolated through the PE matrix in the 5 wt.% FLG-filled PE/PP—60/40 blend composite. Despite lacking the

double percolation effect, this composite presents higher electrical conductivity. In fact, the predominant presence of FLG in the PP phase of the PE/PP blend composite is likely due to the premixing of FLG with the PP phase. Moreover, FLG migration from the PP to PE phase via PE/PP interface is also realized according to thermodynamic prediction [30]. Therefore, thermodynamic preference-induced FLG migration from the PP to PE phase via the PE/PP interface and volume exclusion effect of the PE phase in PE/PP—60/40 and 20/80 blend are two dominant factors in tailoring the conductive FLG network in PE/PP—60/40 and 20/80 blend composites. It has been reported in the literature [50] that once the conductive filler network is fully developed, further addition of filler does not reflect any significant effect on the conductivity of the composite. This phenomenon can be referred to as the saturated effect of the filler network. Moreover, blends with ratios of 60/40 and 20/80 exhibit superior conductivity compared to PE/FLG or PP/FLG composites, even when FLG concentration is higher (9 wt.%). This difference can be attributed to the poor dispersion of FLG in the PE phase compared to the PP phase under the same processing conditions. Moreover, superior electrical conductivity in the PE/PP—60/40 blend composite is not observed when FLG is pre-mixed with PE (see Figure S2 in the Supplementary section). This could be attributed to the possible wrapping of FLG by insulating PE due to a stronger affinity between FLG and PE. Consequently, an interrupted FLG network results in reduced electrical conductivity in PE, even at higher concentrations of FLG. Additionally, during composite cooling, small PE crystals may form on FLG surfaces, impeding FLG contact and resulting in lower electrical conductivity in FLG-filled PE/PP—60/40 blend composites, prepared by FLG premixing with PE phase. These findings underscore the critical role of FLG dispersion and localization in attaining optimal electrical properties in polyolefin blend composites.

Furthermore, the shear-induced deformation applied in the molten condition of the compound does not affect the electrical conductivity of the composite in its solid state. This indicates that the conductive network established by FLG remains unaffected even under applied shear deformation. This highlights the resilience of FLG-filled composites to mechanical deformation while maintaining electrical performance.

FLG addition enhances the tensile modulus of both PE and PP, indicating improved stiffness attributed to the reinforcement effect of FLG. When mechanically strong, rigid fillers are present in polymer-like materials, the fillers act like stress concentrators, facilitating load transfer. In turn, the filler-filled composite increases. Furthermore, better filler-matrix adhesion results in higher strength in the composite. Moreover, FLG incorporation does not adversely affect the impact resistance of the polyolefin blend composites. In general, rigid fillers have two opposing effects on the impact strength of a filler-filled composite. One effect is its role as a defect center, responsible for reducing the impact strength of the composite. Another role is to resist the crack, which is responsible for increasing the impact strength of the composite. When these two effects counterbalance each other, the impact strength of the filler-filled composite may remain unchanged. However, the impact strength of a filler-filled composite can also be influenced by filler-matrix adhesion, filler loading, and the interfacial properties of the composite. The preservation of mechanical properties coupled with the enhancement of stiffness underscores the potential of FLG as a multifunctional filler in polyolefin blend systems. However, the presence of graphene reduced the ductility of the composite, irrespective of the composition of the sample. In general, the presence of rigid particles like few-layer graphene restrains the mobility of polymer chains, which results in a reduction in the ductility of the filler-filled polymer composite.

Furthermore, FLG demonstrates a UV stabilizing effect on polyolefin composites, reducing the formation of carbonyl content, indicative of UV degradation of polymers. Usually, light-absorbing groups (chromophores), as internal or external components in polymer materials, initiate photodegradation [51]. Initially, chromophores absorb photons from UV radiation and become excited. These excited chromophores then break down into free radicals due to further UV exposure in the presence of oxygen. These free radicals attack

the polymer chains and propagate the photodegradation process. The presence of graphene in the polymer matrix can decelerate the photodegradation process by absorbing photons. Additionally, graphene can interact with excited chromophores, absorbing their energy and releasing it as heat, which is known as the quenching effect. Moreover, the π-conjugated electrons in graphene can react with free radicals, neutralizing them and thereby slowing down the photodegradation of the polymer material via the free radical scavenging effect of graphene. Apart from these chemical effects of graphene, it can also act as a physical barrier against oxygen diffusion through the polymer matrix due to its two-dimensional geometry. It has been noticed that the UV stabilizing effect of FLG is more pronounced in PE-rich blends compared to PP-rich blends, highlighting the differential susceptibility of PE and PP to UV degradation. PP exhibits a comparatively higher sensitivity to UV degradation, potentially attributed to the presence of tertiary carbon atoms within the polymer chain [52]. The tertiary carbon atom can be readily attacked by UV radiation, which makes PP more susceptible to UV degradation than PE. The presence of FLG mitigates UV-induced surface cracking and preserves the ductility of the composite materials, further emphasizing its role in enhancing the durability and performance of polyolefin blend composites under UV exposure.

4. Conclusions

This study underscores the notable influence of FLG inclusion on the electrical conductivity, mechanical properties, and UV protection of polyolefin blend composites, as follows:

- The addition of FLG results in electrically conductive, mechanically strong, and more durable PE/PP blend composites.
- The application of shear-induced deformation in molten conditions can change the phase morphology of the blend composite, yet the electrical conductivity remains unaffected, highlighting the resilience of the conductive network within the FLG-filled composites.
- Only 4 wt.% (~2 vol.%) of commercial-grade and low-cost FLG could induce an electrical conductivity of the order of 1.87×10^{-5} S/cm (semi-conductive zone) in PE/PP—60/40.
- As little as 1 wt.% FLG is adequate to retard the UV degradation of polyolefin composite.
- FLG demonstrates a UV stabilizing effect, more pronounced in PE-rich blends, mitigating UV-induced surface cracking and preserving ductility.

In conclusion, FLG offers a versatile solution for designing a reinforced electrostatic dissipative polyolefin composite with improved UV resistance. By understanding the interplay between FLG dispersion, morphology, and filler-polymer interactions, it is possible to tailor the properties of these composites for a variety of applications, from electric applications (semi-conductive separators in power cables, electro-dissipating packaging materials, etc.) to outdoor structural components.

Supplementary Materials: The following supporting information can be downloaded at: https://www.mdpi.com/article/10.3390/cryst14080687/s1. Figure S1: FTIR spectra of neat (a) PE, PE/PP–20/8, PE/PP–60/40 and PP samples, and FTIR spectra of neat (b) PE, (c) PE/PP–20/8, (d) PE/PP–60/40 and (e) PP samples indicating the carbonyl growth after UV exposure within the wave number range of 1680 to 1800 cm^{-1}. Figure S2: Electrical conductivity of PE/PP–60/40 blend composite with 5 wt.% FLG; premixed with PP phase and premixed with PE phase. Figure S3: Distribution of PE droplet size in neat and FLG-filled PE/PP–20/80 blend composite with 1 and 2 wt.% of FLG, respectively, after deformation by 250 strain. Figure S4: SEM image of 2 wt.% FLG-filled PE/PP–20/80 blend composite after deformation, red arrows indicate the deformation-driven migration of FLG from PP phase to PE droplet surface. Figure S5: Tensile strength of PE, PE/PP blends and PP composites as a function of FLG concentration. Figure S6: SEM images of the surface appearance of a polyolefin sample before UV exposure. Table S1: The parameters and corresponding values to calculate the shear rate to ensure droplet coalescence during the coalescence test.

Author Contributions: Conceptualization, S.M.N.S., E.H., G.G., E.D., N.M. and N.R.D.; Methodology, S.M.N.S., E.H., E.D. and N.R.D.; Validation, S.M.N.S., E.H., G.G., E.D., N.M. and N.R.D.; Formal

analysis, S.M.N.S., E.H., G.G., E.D., N.M. and N.R.D.; Investigation, S.M.N.S., E.H., E.D. and N.R.D.; Resources, E.H., G.G., E.D., N.M. and N.R.D.; Writing—original draft, S.M.N.S.; Writing—review and editing, E.H., G.G., E.D., N.M. and N.R.D.; Visualization, S.M.N.S., E.H., E.D. and N.R.D.; Supervision, E.H., G.G., E.D., N.M. and N.R.D.; Project administration, E.H., G.G., E.D., N.M. and N.R.D.; Funding acquisition, S.M.N.S., E.D. and N.R.D. All authors have read and agreed to the published version of the manuscript.

Funding: Grants from NanoXplore Inc.; Natural Sciences and Engineering Research Council (grant number CRDPJ 538482—18); PRIMA Quebec (grant number R18-46-001); Fonds de Recherche du Québec-Nature et Technologies (grant number 318813) were received to conduct the research work. The article processing charge was partially waived by the Editorial Office, MDPI and the rest of the amount funded by the IOAP of Ecole de Technologie Superieure (ETS) Montreal.

Data Availability Statement: The author confirms that the data supporting the reported results can be found within the article and its Supporting Materials. Raw data that supports the findings of this work can be inquired to the corresponding authors, upon reasonable request.

Conflicts of Interest: Author Giovanna Gutiérrez and Nima Moghimian were employed by the company NanoXplore Inc.. The remaining authors declare that the research was conducted in the absence of any commercial or financial relationships that could be construed as a potential conflict of interest.

References

1. Zhu, D.; Bin, Y.; Matsuo, M. Electrical Conducting Behaviors in Polymeric Composites with Carbonaceous Fillers. *J. Polym. Sci. Part B Polym. Phys.* **2006**, *45*, 1037–1044. [CrossRef]
2. dos Anjos, E.G.R.; Marini, J.; Gomes, N.A.S.; Rezende, M.C.; Passador, F.R. Synergistic effect of adding graphene nanoplates and carbon nanotubes in polycarbonate/acrylonitrile-styrene-butadiene copolymer blend. *J. Appl. Polym. Sci.* **2022**, *139*, e52873. [CrossRef]
3. dos Anjos, E.G.; Moura, N.K.; Antonelli, E.; Baldan, M.R.; Gomes, N.A.; Braga, N.F.; Santos, A.P.; Rezende, M.C.; A Pessan, L.; Passador, F.R. Role of adding carbon nanotubes in the electric and electromagnetic shielding behaviors of three different types of graphene in hybrid nanocomposites. *J. Thermoplast. Compos. Mater.* **2022**, *36*, 3209–3235. [CrossRef]
4. Chaudhuri, I.; Fruijtier-Pölloth, C.; Ngiewih, Y.; Levy, L. Evaluating the evidence on genotoxicity and reproductive toxicity of carbon black: A critical review. *Crit. Rev. Toxicol.* **2017**, *48*, 143–169. [CrossRef] [PubMed]
5. Chiu, F.-C.; Behera, K.; Cai, H.-J.; Chang, Y.-H. Polycarbonate/Poly(vinylidene fluoride)-blend-based nanocomposites—Effect of adding different carbon nanofillers/organoclay. *Polymers* **2021**, *13*, 2626. [CrossRef]
6. Nunes, M.A.B.S.; Matos, B.R.; Silva, G.G.; Ito, E.N.; Melo, T.J.A.; Fechine, G.J.M. Hybrids nanocomposites based on a polymer blend (linear low-density polyethylene/poly(ethylene-co-methyl acrylate) and carbonaceous fillers (graphene and carbon nanotube). *Polym. Compos.* **2021**, *42*, 661–677. [CrossRef]
7. López-Martínez, E.D.; Martínez-Colunga, J.G.; Ramírez-Vargas, E.; Sanchez-Valdes, S.; Valle, L.F.R.; Benavides-Cantu, R.; Rodríguez-Gonzalez, J.A.; Mata-Padilla, J.M.; Cruz-Delgado, V.J.; Borjas-Ramos, J.J.; et al. Influence of carbon structures on the properties and photodegradation of LDPE/LLDPE films. *Polym. Adv. Technol.* **2022**, *33*, 1727–1741. [CrossRef]
8. Lago, E.D.; Cagnin, E.; Boaretti, C.; Roso, M.; Lorenzetti, A.; Modesti, M. Influence of different carbon-based fillers on electrical and mechanical properties of a PC/ABS blend. *Polymers* **2020**, *12*, 29. [CrossRef]
9. Cui, Y.; Kundalwal, S.; Kumar, S. Gas barrier performance of graphene/polymer nanocomposites. *Carbon* **2016**, *98*, 313–333. [CrossRef]
10. Afzal, A.; Kausar, A.; Siddiq, M. Perspectives of Polystyrene Composite with Fullerene, Carbon Black, Graphene, and Carbon Nanotube: A Review. *Polym. Technol. Eng.* **2016**, *55*, 1988–2011. [CrossRef]
11. Moghimian, N.; Nazarpour, S. The future of carbon: An update on graphene's dermal, inhalation, and gene toxicity. *Crystals* **2020**, *10*, 718. [CrossRef]
12. Sun, X.; Huang, C.; Wang, L.; Liang, L.; Cheng, Y.; Fei, W.; Li, Y. Recent Progress in Graphene/Polymer Nanocomposites. *Adv. Mater.* **2021**, *33*, e2001105. [CrossRef]
13. Choi, W.; Lahiri, I.; Seelaboyina, R.; Kang, Y.S. Synthesis of graphene and its applications: A review. *Crit. Rev. Solid State Mater. Sci.* **2010**, *35*, 52–71. [CrossRef]
14. Chakraborty, M.; Hashmi, M.S.J. Wonder material graphene: Properties, synthesis and practical applications. *Adv. Mater. Process. Technol.* **2018**, *4*, 573–602. [CrossRef]
15. Ferreira, E.H.C.; Andrade, R.J.E.; Fechine, G.J.M. The "superlubricity state" of carbonaceous fillers on polyethylene-based composites in a molten state. *Macromolecules* **2019**, *52*, 9620–9631. [CrossRef]
16. Karimi, S.; Helal, E.; Gutierrez, G.; Moghimian, N.; David, E.; Samara, M.; Demarquette, N. Photo-stabilization mechanisms of high-density polyethylene (HDPE) by a commercial few-layer graphene. *Polym. Eng. Sci.* **2023**, *63*, 3879–3890. [CrossRef]

17. Abbasi, F.; Shojaei, D.A.; Bellah, S.M. The compatibilization effect of exfoliated graphene on rheology, morphology, and mechanical and thermal properties of immiscible polypropylene/polystyrene (PP/PS) polymer blends. *J. Thermoplast. Compos. Mater.* **2019**, *32*, 1378–1392. [CrossRef]
18. Haghnegahdar, M.; Naderi, G.; Ghoreishy, M.H.R. Electrical and thermal properties of a thermoplastic elastomer nanocomposite based on polypropylene/ethylene propylene diene monomer/graphene. *Soft Mater.* **2017**, *15*, 82–94. [CrossRef]
19. Parameswaranpillai, J.; Joseph, G.; Shinu, K.P.; Jose, S.; Salim, N.V.; Hameed, N. Development of hybrid composites for automotive applications: Effect of addition of SEBS on the morphology, mechanical, viscoelastic, crystallization and thermal degradation properties of PP/PS–xGnP composites. *RSC Adv.* **2015**, *5*, 25634–25641. [CrossRef]
20. Pour, R.H.; Hassan, A.; Soheilmoghaddam, M.; Bidsorkhi, H.C. Mechanical, thermal, and morphological properties of graphene reinforced polycarbonate/acrylonitrile butadiene styrene nanocomposites. *Polym. Compos.* **2016**, *37*, 1633–1640. [CrossRef]
21. Bijarimi, M.; Amirul, M.; Norazmi, M.; Ramli, A.; Desa, M.S.Z.; Desa, A.; Abu Samah, M.A. Preparation and characterization of poly (lactic acid) (PLA)/polyamide 6 (PA6)/graphene nanoplatelet (GNP) blends bio-based nanocomposites. *Mater. Res. Express* **2019**, *6*, 055044. [CrossRef]
22. Rafeie, O.; Aghjeh, M.K.R.; Tavakoli, A.; Kalajahi, M.S.; Oskooie, A.J. Conductive poly(vinylidene fluoride)/polyethylene/graphene blend-nanocomposites: Relationship between rheology, morphology, and electrical conductivity. *J. Appl. Polym. Sci.* **2018**, *135*, 46333. [CrossRef]
23. Sadeghi, A.; Moeini, R.; Yeganeh, J.K. Highly conductive PP/PET polymer blends with high electromagnetic interference shielding performances in the presence of thermally reduced graphene nanosheets prepared through melt compounding. *Polym. Compos.* **2019**, *40*, E1461–E1469. [CrossRef]
24. Al-Saleh, M.H.; Al-Anid, H.K.; Hussain, Y.A. Electrical double percolation and carbon nanotubes distribution in solution processed immiscible polymer blend. *Synth. Met.* **2013**, *175*, 75–80. [CrossRef]
25. Sumita, M.; Sakata, K.; Hayakawa, Y.; Asai, S.; Miyasaka, K.; Tanemura, M. Double percolation effect on the electrical conductivity of conductive particles filled polymer blends. *Colloid Polym. Sci.* **1992**, *270*, 134–139. [CrossRef]
26. Jia, L.; Yan, D.; Cui, C.; Ji, X.; Li, Z. A Unique double percolated polymer composite for highly efficient electromagnetic interference shielding. *Macromol. Mater. Eng.* **2016**, *301*, 1232–1241. [CrossRef]
27. Otero-Navas, I.; Arjmand, M.; Sundararaj, U. Carbon nanotube induced double percolation in polymer blends: Morphology, rheology and broadband dielectric properties. *Polymer* **2017**, *114*, 122–134. [CrossRef]
28. Pan, Y.; Liu, X.; Hao, X.; Starý, Z.; Schubert, D.W. Enhancing the electrical conductivity of carbon black-filled immiscible polymer blends by tuning the morphology. *Eur. Polym. J.* **2016**, *78*, 106–115. [CrossRef]
29. Strugova, D.; Junior, J.C.F.; David, É.; Demarquette, N.R. Ultra-low percolation threshold induced by thermal treatments in co-continuous blend-based PP/PS/MWCNTs nanocomposites. *Nanomaterials* **2021**, *11*, 1620. [CrossRef]
30. Tu, C.; Nagata, K.; Yan, S. Influence of melt-mixing processing sequence on electrical conductivity of polyethylene/polypropylene blends filled with graphene. *Polym. Bull.* **2017**, *74*, 1237–1252. [CrossRef]
31. Bouhfid, R.; Arrakhiz, F.; Qaiss, A. Effect of graphene nanosheets on the mechanical, electrical, and rheological properties of polyamide 6/Acrylonitrile–Butadiene–Styrene blends. *Polym. Compos.* **2016**, *37*, 998–1006. [CrossRef]
32. Wang, F.; Zhang, Y.; Zhang, B.; Hong, R.; Kumar, M.; Xie, C. Enhanced electrical conductivity and mechanical properties of ABS/EPDM composites filled with graphene. *Compos. Part B Eng.* **2015**, *83*, 66–74. [CrossRef]
33. Graziano, A.; Garcia, C.; Jaffer, S.; Tjong, J.; Yang, W.; Sain, M. Functionally tuned nanolayered graphene as reinforcement of polyethylene nanocomposites for lightweight transportation industry. *Carbon* **2020**, *169*, 99–110. [CrossRef]
34. Graziano, A.; Garcia, C.; Jaffer, S.; Tjong, J.; Sain, M. Novel functional graphene and its thermodynamic interfacial localization in biphasic polyolefin systems for advanced lightweight applications. *Compos. Sci. Technol.* **2020**, *188*, 107958. [CrossRef]
35. Zhong, Y.L.; Tian, Z.; Simon, G.P.; Li, D. Scalable production of graphene via wet chemistry: Progress and challenges. *Mater. Today* **2015**, *18*, 73–78. [CrossRef]
36. Moghimian, N.; Saeidlou, S.; Lentzakis, H.; Rosi, G.F.; Song, N.; David, E. Electrical conductivity of commercial graphene polyethylene nanocomposites. In Proceedings of the 2017 IEEE 17th International Conference on Nanotechnology (IEEE-NANO), Pittsburgh, PA, USA, 25–28 July 2017; pp. 757–761.
37. Aprianti, N.; Kismanto, A.; Supriatna, N.K.; Yarsono, S.; Nainggolan, L.M.T.; Purawiardi, R.I.; Fariza, O.; Ermada, F.J.; Zuldian, P.; Raksodewanto, A.A.; et al. Prospect and challenges of producing carbon black from oil palm biomass: A review. *Bioresour. Technol. Rep.* **2023**, *23*, 101587. [CrossRef]
38. Batista, N.L.; Helal, E.; Kurusu, R.S.; Moghimian, N.; David, E.; Demarquette, N.R.; Hubert, P. Mass-produced graphene—HDPE nanocomposites: Thermal, rheological, electrical, and mechanical properties. *Polym. Eng. Sci.* **2019**, *59*, 675–682. [CrossRef]
39. Singh, M.K.; Mohanty, A.K.; Misra, M. Upcycling of waste polyolefins in natural fiber and sustainable filler-based biocomposites: A study on recent developments and future perspectives. *Compos. Part B Eng.* **2023**, *263*, 110852. [CrossRef]
40. Karlsson, S. Recycled polyolefins. Material properties and means for quality determination. *Adv. Polym. Sci.* **2004**, *169*, 201–229. [CrossRef]
41. Vandebril, S.; Vermant, J.; Moldenaers, P. Efficiently suppressing coalescence in polymer blends using nanoparticles: Role of interfacial rheology. *Soft Matter* **2010**, *6*, 3353–3362. [CrossRef]
42. Thareja, P.; Moritz, K.; Velankar, S.S. Interfacially active particles in droplet/matrix blends of model immiscible homopolymers: Particles can increase or decrease drop size. *Rheol. Acta* **2010**, *49*, 285–298. [CrossRef]

43. Grace, H.P. Dispersion phenomena in high viscosity immiscible fluid systems and application of static mixers as dispersion devices in such systems. *Chem. Eng. Commun.* **1982**, *14*, 225–277. [CrossRef]
44. Tucker, C.L., III; Moldenaers, P. Microstructural evolution in polymer blends. *Annu. Rev. Fluid Mech.* **2002**, *34*, 177–210. [CrossRef]
45. Graziano, A.; Dias, O.A.T.; Garcia, C.; Jaffer, S.; Tjong, J.; Sain, M. Impact of Reduced Graphene Oxide on structure and properties of polyethylene rich binary systems for performance-based applications. *Polymer* **2020**, *202*, 122622. [CrossRef]
46. Strugova, D.; David, É.; Demarquette, N.R. Effect of steady shear deformation on electrically conductive PP/PS/MWCNT composites. *J. Rheol.* **2023**, *67*, 977–993. [CrossRef]
47. Guo, Y.; Zuo, X.; Xue, Y.; Tang, J.; Gouzman, M.; Fang, Y.; Zhou, Y.; Wang, L.; Yu, Y.; Rafailovich, M.H. Engineering thermally and electrically conductive biodegradable polymer nanocomposites. *Compos. Part B Eng.* **2020**, *189*, 107905. [CrossRef]
48. Parameswaranpillai, J.; Sanjay, M.; Varghese, S.A.; Siengchin, S.; Jose, S.; Salim, N.; Hameed, N.; Magueresse, A. Toughened PS/LDPE/SEBS/xGnP ternary composites: Morphology, mechanical and viscoelastic properties. *Int. J. Light. Mater. Manuf.* **2019**, *2*, 64–71. [CrossRef]
49. Juan, L. Simultaneous improvement in the tensile and impact strength of polypropylene reinforced by graphene. *J. Nanomater.* **2020**, *2020*, 7840802. [CrossRef]
50. Arjmand, M.; Apperley, T.; Okoniewski, M.; Sundararaj, U. Comparative study of electromagnetic interference shielding properties of injection molded versus compression molded multi-walled carbon nanotube/polystyrene composites. *Carbon* **2012**, *50*, 5126–5134. [CrossRef]
51. Karimi, S.; Helal, E.; Gutierrez, G.; Moghimian, N.; Madinehei, M.; David, E.; Samara, M.; Demarquette, N. A review on graphene's light stabilizing effects for reduced photodegradation of polymers. *Crystals* **2021**, *11*, 3. [CrossRef]
52. Gijsman, P.; Meijers, G.; Vitarelli, G. Comparison of the UV-degradation chemistry of polypropylene, polyethylene, polyamide 6 and polybutylene terephthalate. *Polym. Degrad. Stab.* **1999**, *65*, 433–441. [CrossRef]